Intraflagellar transport particle size scales inversely with flagellar length: revisiting the balance-point length control model

Benjamin D. Engel, William B. Ludington, and Wallace F. Marshall

Department of Biochemistry and Biophysics, University of California, San Francisco, San Francisco, CA 94158

The assembly and maintenance of eukaryotic flagella are regulated by intraflagellar transport (IFT), the bidirectional traffic of IFT particles (recently renamed IFT trains) within the flagellum. We previously proposed the balance-point length control model, which predicted that the frequency of train transport should decrease as a function of flagellar length, thus modulating the length-dependent flagellar assembly rate. However, this model was challenged by the differential interference contrast microscopy observation that IFT frequency is length independent. Using total internal reflection fluorescence microscopy to quantify protein traffic during the regeneration of *Chlamydomonas reinhardtii* flagella, we determined that anterograde IFT trains in short flagella are composed of more kinesin-associated protein and IFT27 proteins than trains in long flagella. This length-dependent remodeling of train size is consistent with the kinetics of flagellar regeneration and supports a revised balance-point model of flagellar length control in which the size of anterograde IFT trains tunes the rate of flagellar assembly.

Introduction

How cells regulate organelle size is a fundamental question in cell biology. The eukaryotic flagellum (a term used interchangeably with cilium), with its easily measured linear geometry, provides an ideal model for studying organelle size control. Furthermore, ciliary length control has become increasingly medically relevant, with recent studies linking ciliary defects to a wide range of human disorders (Pazour and Rosenbaum, 2002; Bisgrove and Yost, 2006).

The unicellular biflagellate green alga *Chlamydomonas reinhardtii* is a powerful tool for studying flagellar biology (Randall et al., 1969; Silflow and Lefebvre, 2001). After abscission, flagella regenerate to their original length with reproducible kinetics (Fig. 1 A). Short flagella undergo a period of rapid growth then transition to a slow elongation phase as they near their steady-state length (Fig. 1 B). Although this phenomenon was first observed 40 yrs ago (Rosenbaum et al., 1969), the mechanisms that control the kinetics of flagellar regeneration are not well understood. Studies in *C. reinhardtii* have revealed that the assembly and maintenance of flagella depend on intraflagellar transport (IFT), the molecular motor-driven process of bidirectional protein traffic within the flagellum (Kozminski et al., 1993). IFT describes the movement of IFT trains (previously referred to as "particles" but renamed "trains" based on electron tomography; Pigino et al., 2009), heterogeneous linear protein arrays composed of heterotrimeric kinesin-2, cytoplasmic dynein-1b, axonemal cargo, and two varieties of IFT complexes (A and B; Piperno and Mead, 1997; Cole et al., 1998; Cole, 2003; Ou et al., 2007). Kinesin powers anterograde transport to the distal tip of the flagellum, where the trains are remodeled and subsequently undergo dynein-driven retrograde return to the base. IFT has been shown to be directly responsible for the transport of axonemal precursors to the site of flagellar assembly at the tip (Qin et al., 2004; Hou et al., 2007). Defects in kinesin, dynein, and most of the IFT proteins all lead to short or absent flagella (Huang et al., 1977; Piperno et al., 1998; Pazour et al., 1999, 2000; Porter et al., 1999; Deane et al., 2001; Pedersen et al., 2005). Additionally, reducing the speed and frequency of IFT leads to flagellar shortening (Kozminski et al., 1995; Iomini et al., 2001). Thus, IFT appears to play a central role in mediating flagellar length.

B.D. Engel and W.B. Ludington contributed equally to this paper.

Correspondence to Wallace F. Marshall: wallace.marshall@biochem.ucsf.edu

Abbreviations used in this paper: CCD, charge-coupled device; DIC, differential interference contrast; IFT, intraflagellar transport; KAP, kinesin-associated protein; ROI, region of interest; TAP, Tris-acetate-phosphate; TIRF, total internal reflection fluorescence.

The Rockefeller University Press $30.00
J. Cell Biol. Vol. 187 No. 1 81–89
www.jcb.org/cgi/doi/10.1083/jcb.200812084

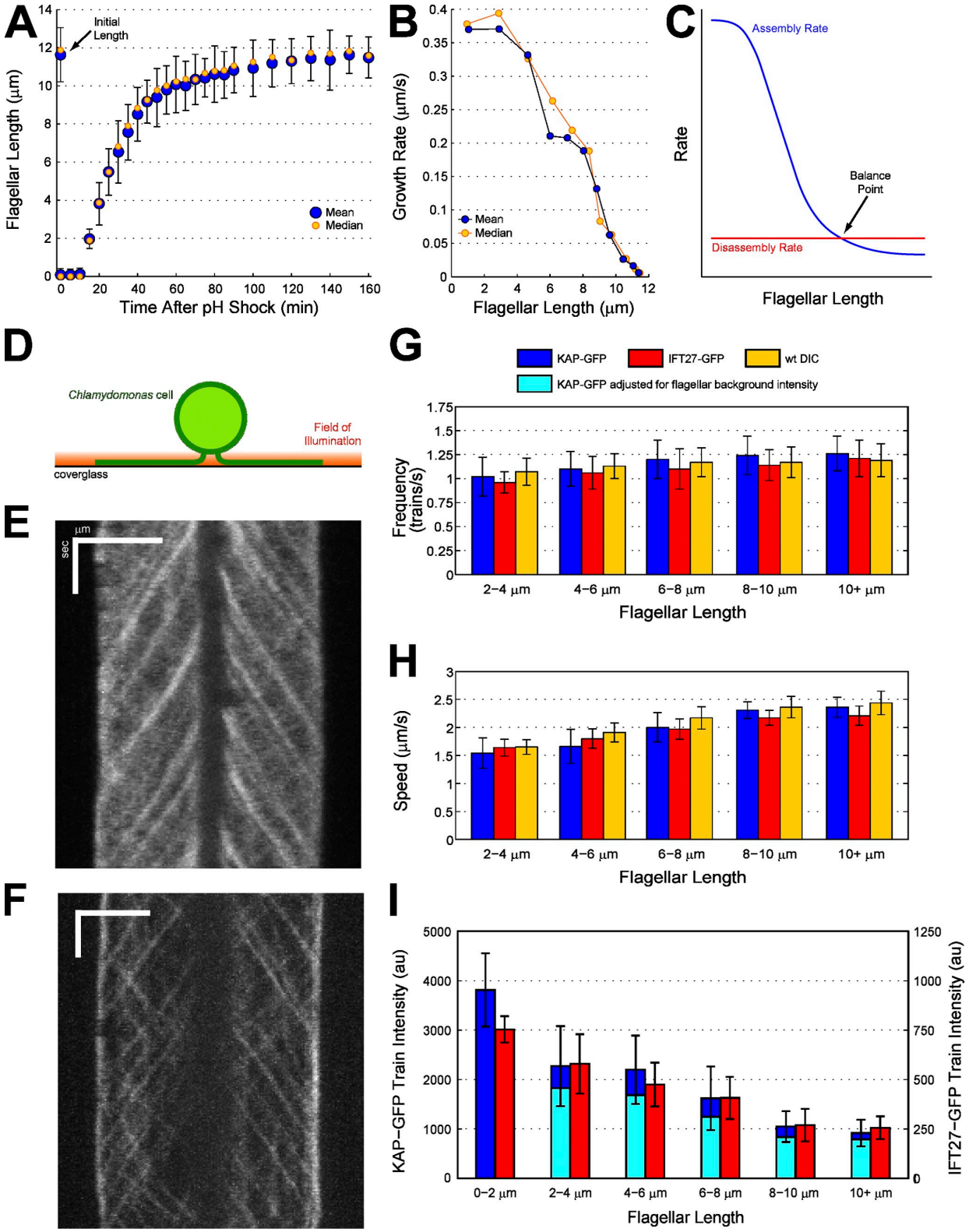

Figure 1. **During flagellar regeneration, there is an inverse relationship between IFT train size and flagellar length.** (A) The kinetics of regeneration after pH shock. *n* for all time points combined = 2,026 flagella. (B) The growth rate of regenerating flagella decreases as a function of length. (C) The balance-point model predicts that equilibrium will be reached between a length-independent disassembly rate and an assembly rate that decreases as a function of length. (D) The setup for imaging *C. reinhardtii* flagella via TIRF. (E and F) Kymographs of KAP-GFP (E) and IFT27-GFP (F) cells undergoing regeneration after pH shock, generated from Videos 1 and 2. Bars: (horizontal) 5 μm; (vertical) 1 s. (G–I) The frequency (G), speed (H), and average (I) intensity of IFT trains during pH shock regeneration, binned by flagellar length. The intensities of IFT traces were normalized by either camera noise (dark blue and red bars) or background flagellar intensity (light blue bars). *n* for all time points = 113 KAP-GFP flagella, 97 IFT27-GFP flagella, and 97 wild-type (wt) flagella imaged by DIC. Error bars indicate standard deviation.

The balance-point model of flagellar length control (Fig. 1 C; Marshall and Rosenbaum, 2001; Marshall et al., 2005) proposes that flagellar length is the resultant of two opposing rates: a length-independent disassembly rate and an assembly rate that decreases as the flagellum elongates. The length-independent disassembly rate is supported by the observation that when IFT is stopped in the *fla10*-conditional kinesin-2 mutant, disassembly occurs at a constant basal rate regardless of flagellar length (Kozminski et al., 1995; Marshall and Rosenbaum, 2001; Parker and Quarmby, 2003; Marshall et al., 2005). Furthermore, during drug- or mitosis-induced active flagellar disassembly, a process that requires retrograde IFT, flagella also shorten at a length-independent rate (Marshall et al., 2005; Pan and Snell, 2005). The balance-point model predicts that the flagellar assembly rate decreases as a function of length until the flagellum reaches a unique steady-state length in which the assembly and disassembly rates are in equilibrium. Driven by the observation that short and long flagella contain roughly the same quantity of IFT protein (Marshall et al., 2005), the original balance-point model proposed that the number of IFT trains in a flagellum is constant. Thus, the length-dependent assembly rate would arise from the variable frequency of anterograde trafficking events. As the flagellum lengthens, trains would become spaced further apart, new cargo would arrive at the tip less frequently, and the assembly rate would decrease (see Fig. 4 A).

However, experiments using differential interference contrast (DIC) microscopy revealed that long flagella actually contain more IFT trains than short flagella (Dentler, 2005). This observation appears to invalidate a key prediction of the balance-point model and seems to be inconsistent with the finding that all flagella contain the same amount of IFT protein. However, this conflict is based on the assumption that all trains are equivalently sized. In fact, IFT trains have been demonstrated to be modular. When viewed by transmission EM, trains range from 100 to >600 nm in length (Pedersen et al., 2006) and are composed of a variable number of smaller, linearly arranged particle substructures (Kozminski et al., 1993, 1995; Pigino et al., 2009). Furthermore, immunogold localization experiments suggest that the number of IFT proteins in a train can vary by severalfold (Sloboda and Howard, 2007). Thus, changes in IFT train size, rather than frequency, could theoretically mediate the length-dependent assembly rate predicted by the balance-point model.

Results and discussion

To test the predictions of the revised balance-point model, we needed an accurate method to assay IFT train size in live cells undergoing flagellar regeneration. Previous attempts to visualize IFT in *C. reinhardtii* have primarily relied on DIC microscopy. Although this technique can measure the speed and frequency of IFT (Kozminski et al., 1993; Iomini et al., 2001; Dentler, 2005), it is insufficient for quantifying train size. The apparent size of trains seen by DIC is not a good measure of protein content, as it is affected by the angle of DIC shear and the train's refractive index. We decided instead to use fluorescence microscopy to quantify the amount of GFP-labeled IFT protein found in each train. GFP tagging of IFT proteins has been extensively used in *Caenorhabditis elegans* (Orozco et al., 1999; Ou et al., 2007), but *C. reinhardtii* provides a significant advantage for visualizing IFT. Because wild-type *C. reinhardtii* cells adhere both their flagella to the cover glass (Bloodgood, 1995), we were able to achieve high fidelity measurements with adjusted total internal reflection fluorescence (TIRF; Axelrod, 2001; Mattheyses and Axelrod, 2006), where the angle of incident light is decreased to close to the critical angle, providing a deeper field of illumination near the cover glass (250–350 nm; see Materials and methods). Using this setup (Fig. 1 D), we imaged completely through adhered flagella (Fig. S1 A) at ∼30 frames per second, whereas the autofluorescent cell bodies remained outside the field of illumination.

We analyzed two key members of anterograde trains: kinesin-associated protein (KAP; Mueller et al., 2005), the nonmotor subunit of kinesin-2, and IFT27 (Qin et al., 2007), a small Rab-like GTPase that is a core component of IFT complex B. IFT complex B is required for anterograde transport and is thought to be present in every anterograde train. By making kymographs from videos of KAP-GFP and IFT27-GFP strains (Fig. 1, E and F; and Videos 1 and 2), we extracted information about the speed, frequency, and GFP intensity of IFT trains (Fig. S1 B). We restricted our analysis to anterograde IFT because it is these trains that contribute to the length-dependent rate of axoneme assembly. Retrograde IFT may contribute to disassembly, but it appears to do so in a length-independent manner (Pan and Snell, 2005), which cannot explain the kinetics of flagellar regeneration and the steady-state length.

To observe how IFT is affected by flagellar regeneration, we exposed cells to an acidic pH shock, which induces flagellar abscission (Lefebvre, 1995). During the subsequent regeneration phase, we measured the speed, frequency, and GFP intensity of anterograde transport and correlated these measurements with flagellar length. Consistent with previous observations (Dentler, 2005), we found that anterograde IFT frequency is relatively length independent and varies between ∼1 train per second in short flagella to ∼1.25 trains per second in long flagella (Fig. 1 G). Short flagella exhibited more variable and reduced anterograde IFT speeds, averaging ∼1.6 µm per second, whereas trains in long flagella had a consistent top speed of ∼2.3 µm per second (Fig. 1 H). However, reduced anterograde speeds in short flagella cannot explain the increased assembly rate predicted by the balance-point model. Correlating the GFP intensity of anterograde traces with flagellar length revealed an intriguing relationship: IFT trains in short flagella (2–6 µm) were over twice as intense as those in long flagella (≥8 µm; Fig. 1 I). Furthermore, trains in flagella that were too short to distinguish individual trafficking events (<2 µm) were three to four times as bright as trains in long flagella. Because GFP intensity serves as a proxy for GFP number, we concluded that IFT trains in short flagella contained severalfold more KAP-GFP and IFT27-GFP proteins. Thus, trains in short flagella are functionally larger with a greater cargo-carrying capacity. Although IFT27-GFP had a very low flagellar background signal that was comparable with the camera noise (Fig. 1 F), KAP-GFP had significantly higher background intensity that was brightest in short regenerating flagella (Fig. 1 E). However, even

when normalized by this background signal, trains in short flagella were over twice as intense as trains in long flagella (Fig. 1 I, light blue bars). Because train traffic could not be distinguished in very short flagella (<2 µm), the flagellar background was not measurable.

Although IFT frequency and particularly IFT speed were reduced in regenerating short flagella, both parameters were uncorrelated with train intensity (Fig. S2, A and B). This means that although slow and large trains are both found in short flagella, large trains are not predisposed to being slow. However, we did uncover a moderate length-independent correlation between IFT speed and frequency, which was strongest within the KAP-GFP dataset (Fig. S2 C).

To confirm that trains in short flagella contained more KAP protein, we fixed KAP-GFP cells at various time points after pH shock and quantified the number of GFP molecules in each train by counting stepwise photobleaching events under TIRF illumination (Fig. 2; Leake et al., 2006). We chose to focus on the KAP-GFP strain for this experiment because it was created in an *fla3* (KAP point mutant) background in which only exogenously expressed KAP protein enters the flagella (Fig. S1 C; Mueller et al., 2005). Thus, every KAP protein in the trains is GFP labeled. However, the IFT27-GFP strain has a mixture of endogenous and labeled protein in its flagella (Qin et al., 2007). Throughout the time course of the bleach, the average fluorescence was measured in regions of interest (ROIs) corresponding to spots of peak intensity (IFT trains) along the flagella (Fig. 2 A). Fluorescence in each ROI was lost in an exponential and stepwise manner, and many steps fit a relatively uniform size (25–60 counts, depending on the imaging session), which is consistent with single GFP bleaching events (Fig. 2 B). Before quantification, the steps were enhanced with an edge-preserving Chung-Kennedy filter (Fig. 2 B, blue; Chung and Kennedy, 1991; Smith, 1998; Leake et al., 2006). Much like the live cell experiments, we found that trains in short flagella were enriched with severalfold more KAP-GFP proteins. Trains in long flagella contained an average of six KAP-GFP proteins, trains in half-length flagella possessed an average of 10 KAP-GFP, and trains in short flagella held an average of 16 KAP-GFP (Fig. 2 C). ROIs in very short flagella (<2 µm) routinely had >20 KAP-GFP proteins. Strikingly, this length-dependent two- to fourfold difference in KAP-GFP protein number mirrors the two- to fourfold difference in train intensity seen in Fig. 1. Step totals counted by eye were confirmed by dividing the total bleached intensity by the average GFP step size determined for each trace. The tight correlation between the number of GFP steps and the total bleached intensity for each ROI (Fig. S1 D) suggests not only that GFP number was accurately quantified but also that GFP intensity (as reported in Fig. 1) is indeed a strong proxy for GFP protein content.

Although these initial studies revealed the relationship between train size and flagellar length, both experiments were susceptible to variability as a result of comparing data from different images (variability in laser intensity and alignment) of different cells within a population (intrinsic cell to cell variability in IFT pool size and GFP expression levels). Fortunately, we were able to address these concerns thanks to a unique *C. reinhardtii* behavior known as the long-zero response, which occurs when only one of the flagella is severed. During the ∼30 min after abscission, the two flagella equilibrate in length by shortening the long flagellum as the severed flagellum grows (Rosenbaum et al., 1969). This experiment provides an elegant, internally controlled opportunity to use a single image to compare the IFT dynamics between a long flagellum and short flagellum, both of which are sharing the same limited pool of IFT proteins. When we began our long-zero observations, it was immediately apparent that the shorter flagellum contained trains with higher GFP intensity. Furthermore, greater differences in length between the flagella were accompanied by greater differences in train intensity (Fig. 3, A and B; and Videos 3–6). Quantification revealed a 1:1 linear correlation between train intensity and flagellar length. For example, a flagellum that was half the length of its counterpart would have trains that were twice as bright (Fig. 3 C shows a subset of the data with a length ratio <4, corrected for flagellar background; Fig. S3 shows the complete dataset, corrected for camera noise). In contrast, the speed and frequency of IFT were similar in both flagella regardless of the difference in lengths (Fig. 3, D and E). Based on the pH shock experiment, we expected long flagella to have slightly faster IFT than short flagella, but surprisingly, the speeds in long flagella were often reduced (<2 µm/s). This could be a unique feature of long zeros, or more generally, a feature of all rapidly shortening flagella.

We also found that, with the exception of long zeros with one very short flagellum (length ratio >4), both flagella contained roughly the same amount of total integrated fluorescence (intensity ratio of ∼1; Fig. S3 A). This supports the claim that short and long flagella contain the same quantity of IFT protein (Marshall et al., 2005), and along with the constant frequency of IFT and the linear relationship between train size and flagellar length, suggests a "conservation of mass" in the IFT system. As flagella regenerate, a fixed length-independent quantity of IFT protein is redistributed from fewer large trains to a greater number of small trains (Fig. 4 A). Although the mechanism is different than what was originally proposed in the balance-point model, the model's central dogma remains unchanged. Lengthening of the flagellum results in a lower local concentration of IFT material and axonemal precursors at the flagellar tip, and thus, a lower assembly rate.

It will be of great interest to see whether all IFT proteins scale stoichiometrically with KAP and IFT27 or whether certain proteins demonstrate a fixed quantity per train, regardless of length. Initial studies of IFT20-GFP (provided by K. Lechtreck and G. Witman, University of Massachusetts, Worcester, MA), a peripheral IFT complex B subunit believed to link kinesin with complex B (Baker et al., 2003), indicate that IFT20 train content also scales inversely with flagellar length (unpublished data). Our current balance-point model makes the key assumption that all IFT trains carry a proportionate quantity of cargo. This is hard to test directly because the GFP signal of a labeled cargo would be lost in the signal from cargo that has already been incorporated into the axoneme. Nevertheless, a "regulated cargo loading" model has been proposed in which some IFT trains are incapable of binding cargo (Snell et al., 2004).

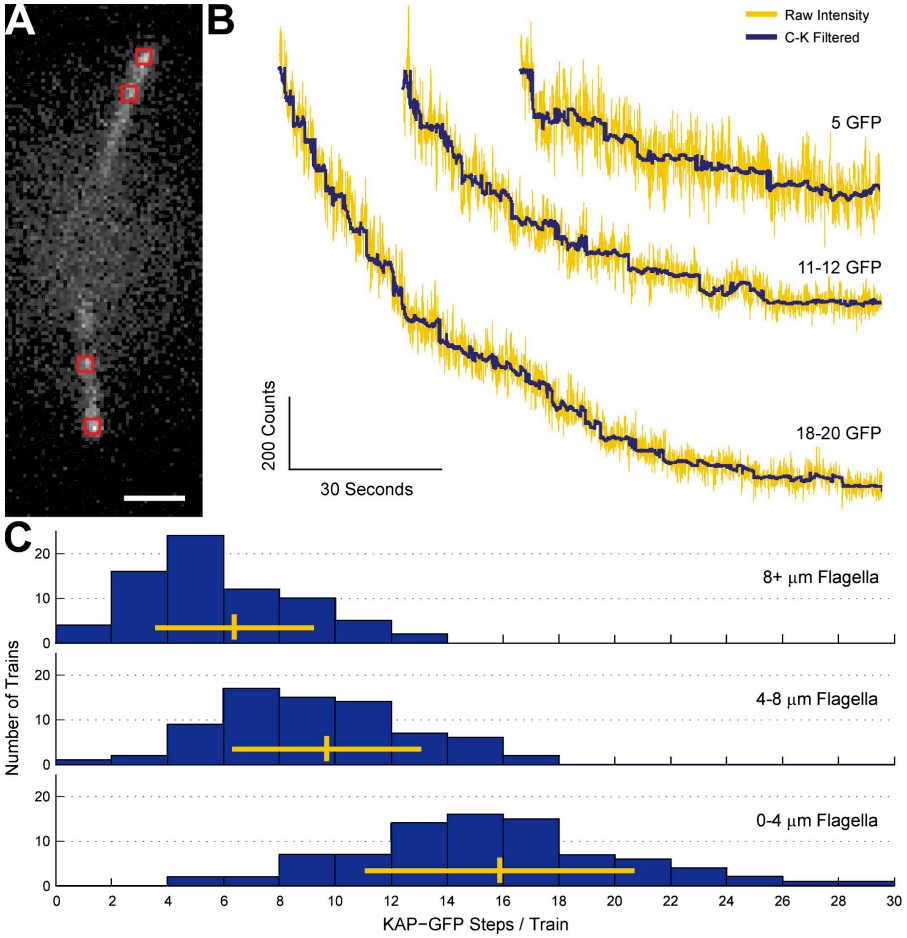

Figure 2. **Quantitative photobleaching confirms that IFT trains in short flagella contain more KAP protein.** (A) At different time points after pH shock, KAP-GFP cells were for fixed and photobleached under constant TIRF illumination. The mean intensity was measured from 0.4 × 0.4 μm ROIs (red squares) centered on IFT trains. Bar, 2 μm. (B) Three examples of intensity plots of ROIs from flagella of different lengths. The raw data were filtered with a Chung-Kennedy edge-preserving algorithm to enhance the detection of stepwise GFP bleaching events. (C) Histograms of the number of KAP-GFP proteins measured in ROIs from long, mid-length, and short flagella (yellow vertical bars denote the mean, yellow horizontal bars show the standard deviation). *n* = 230 ROIs from 90 flagella.

Another assumption in the balance-point model is that IFT train speed is length independent. Our data shows that this is not strictly true, as short flagella in the pH shock experiment have reduced IFT speeds (Fig. 1 H). However, a modified mathematical model that incorporates this speed variation shows that the measured speeds do not affect the ability of the balance-point system to maintain a defined length (unpublished data).

The mechanisms that cause train size to scale inversely with flagellar length remain to be determined. Two distinct models could theoretically explain this behavior: a closed self-rectifying system or an open system with a length sensor (Fig. 4 B). In a self-rectifying system, flagellar length control is independent of an additional signaling mechanism. Under this regimen, the amount of IFT protein available for anterograde train assembly is dependent on the amount of material returned to the base of the flagellum by retrograde transport. As the flagellum lengthens, less IFT components are available at the base of the flagellum, and anterograde train size decreases. This model relies on the flagellum being a relatively closed system (no cytoplasmic exchange) for at least one key component of the IFT machinery. In a completely open system, the flagellum would require a length senor to modulate the input size of IFT trains. Length sensors could detect a signal from the flagellar tip, react to changes in ion concentration from channels in the flagellar membrane (Rosenbaum, 2003), or act via a time of flight mechanism that would translate the transport time of a trafficking signaling protein (such as a GTPase or kinase) into length measurements (Sloboda and Rosenbaum, 2007). Although several proteins have been shown to play a role in length regulation, including the flagellar localized kinases GSK3, LF4p, and Cnk2p (Berman et al., 2003; Wilson and Lefebvre, 2004; Bradley and Quarmby, 2005), a specific length-sensing mechanism has yet to be demonstrated. Differentiating between open and closed flagellar systems would benefit greatly from a *C. reinhardtii* codon-optimized photoactivatable GFP (Patterson and Lippincott-Schwartz, 2002).

An interesting observation that deserves additional investigation is the apparent lack of KAP-GFP retrograde transport. Although kymographs of IFT27-GFP (Fig. 1 F) and IFT20-GFP (not depicted) have a low background signal and frequent bright retrograde traces, KAP-GFP kymographs have higher background and retrograde traces that are infrequent and far less intense than anterograde traces (Fig. 1 E). The lack of bright retrograde KAP-GFP traces is consistent with the observation in *fla11* (IFT172) mutants that kinesin can exit flagella independent of IFT (Pedersen et al., 2006). Without photoactivation, we cannot currently distinguish whether retrograde KAP is undergoing diffusion or whether it is transported back to the base as single molecules obscured from detection by the flagellar noise. If kinesin does detach from IFT trains at the flagellar tip, this suggests a model for the turnaround of IFT trains where kinesin inhibits dynein during anterograde transport,

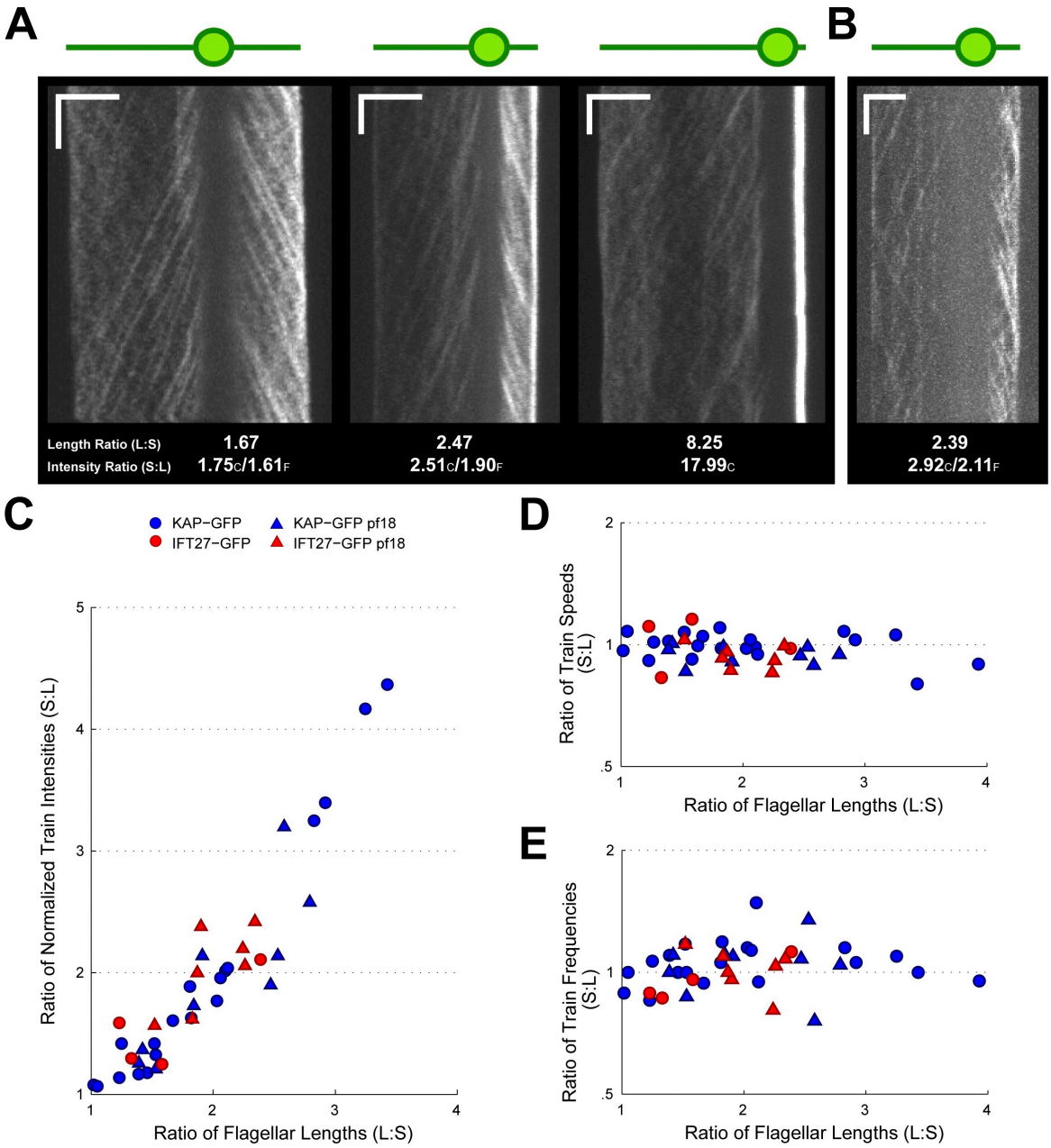

Figure 3. **During long-zero regeneration, there is a linear correlation between IFT train size and flagellar length.** (A) Three examples of KAP-GFP cells undergoing long-zero regeneration, showing brighter IFT trains in the shorter of the two flagella (cell dimensions are diagramed above the kymographs). As the length disparity between the long and short flagella increases (kymographs left to right), the difference in average train intensity also increases. Kymographs were generated from Videos 3–5. (B) Example of an IFT27-GFP long-zero cell. Kymograph was generated from Video 6. (A and B) Bars: (horizontal) 5 µm; (vertical) 1 s. (C) Plotting data from all of the KAP-GFP and IFT27-GFP long-zero cells together reveals a linear relationship (r^2 = 0.86) between the ratio of flagellar lengths and the ratio of IFT train intensities. Train intensities were corrected for the flagellar background and normalized by the ratio of integrated flagellar intensities (Fig. S3 B) to control for variability in total IFT content. (D and E) Despite this correlation between length and train intensity, the speed (D) and frequency (E) of IFT is the same in both the long and short flagella. (C–E) Data are plotted on a ratio scale. S, short flagella; L, long flagella, C, corrected for camera noise; F, corrected for flagellar background.

either through pulling forces alone (Müller et al., 2008) or through protein interactions (Deacon et al., 2003). At the tip, kinesin is removed from IFT trains, immediately licensing dynein for retrograde transport. Such a model would predict a rapid turnaround of trains at the flagellar tip, a premise that can also be tested with photoactivation.

In summary, we have observed that the size of IFT trains in regenerating *C. reinhardtii* flagella scales inversely and linearly as a function of flagellar length. This provides a plausible mechanism to support the balance-point model of flagellar length control. Based on our observations, we propose that the redistribution of a fixed quantity of IFT protein into IFT trains of variable size drives the length-dependent assembly rate and thus the kinetics of flagellar regeneration and the steady-state flagellar length. It will be of great interest to see whether IFT is altered in the extensive catalog of *C. reinhardtii* mutants that

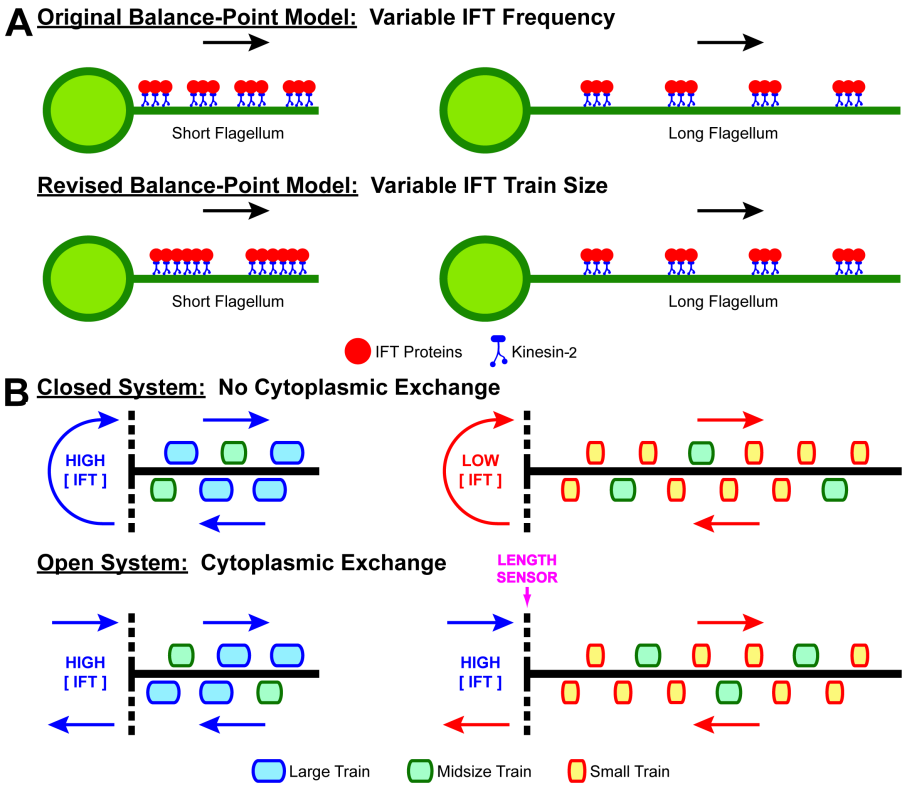

Figure 4. **The original and revised balance-point models of flagellar length control and possible mechanisms of IFT train size modulation.** (A) The original balance-point model predicted that flagella contain a fixed number of IFT trains. Thus, as flagella regenerate, the length-dependent assembly rate would be driven by the decreasing frequency of train arrival at the flagellar tip. This model was refuted by the DIC observation that IFT frequency is constant (Dentler, 2005). In the revised model, the length-dependent assembly rate is mediated by IFT train size that scales inversely with flagellar length. Although the total amount of kinesin-2 and IFT protein in a flagellum is length independent, these proteins are redistributed into a greater number of smaller trains as the flagellum regenerates, reducing the rate of flagellar assembly. (B) Two possible models of train size control. In a closed system, at least one essential component of the IFT machinery does not exchange freely with the cytoplasmic pool. As the flagellum lengthens, lower concentrations of this key protein arrive at the flagellar base via retrograde transport, which results in the production of smaller anterograde IFT trains. In an open system, there is always a high availability of IFT material at the flagellar base, as proteins freely exchange with the large cytoplasmic pool. Thus, an additional length-sensor mechanism is required to modulate the size of trains that enter the flagellum. Blue arrows indicate high IFT protein concentration, whereas red arrows indicate low concentration.

exhibit abnormally long (*lf*) or short (*shf*) flagellar lengths (Kuchka and Jarvik, 1987; Asleson and Lefebvre, 1998). It will also be informative to determine how IFT scales with flagellar length in other model systems such as *Trypanosoma brucei*, *Tetrahymena thermophila*, *C. elegans*, and vertebrates, all of which have established GFP reporter systems for observing IFT in live cells (Orozco et al., 1999; Follit et al., 2006; Absalon et al., 2008; Tsao and Gorovsky, 2008). Although perhaps not as perfectly suited to studying flagellar regeneration, each of these organisms presents unique characteristics (e.g., two flagella of unequal length and age in *T. brucei*) that may provide additional insights into the relationship between IFT and flagellar length.

Materials and methods

Strains and culture conditions

Vegetative *C. reinhardtii* cells were grown in Tris-acetate-phosphate (TAP) media (Gorman and Levine, 1965) at 21°C with constant aeration. Wild-type mt+ (cc125), *pf18* mt+ (cc1036), and *pf18* mt− (cc1297) strains were obtained from the *Chlamydomonas* Genetics Center (Duke University, Durham, NC). KAP-GFP *fla3* mt− (Mueller et al., 2005), IFT27-GFP mt+ (Qin et al., 2007), and IFT20-GFP ΔIFT20 (provided by K. Lechtreck) strains were provided by M. Porter (University of Minnesota, Minneapolis, MN), J. Rosenbaum (Yale University, New Haven, CT), and G. Witman (University of Massachusetts Medical School, Worcester, MA), respectively. KAP-GFP *fla3 pf18*, IFT27-GFP *pf18*, and KAP-GFP (wild-type *fla3* allele) strains were generated through crosses. All constructs used *C. reinhardtii* codon-optimized GFP (Fuhrmann et al., 1999).

pH shock was performed by transiently lowering the pH of *C. reinhardtii* cultures as previously described (Lefebvre, 1995). Long-zero regeneration was induced by passing cells through a 28-gauge insulin needle (Micro-Fine; BD), which sheared off only one of the two flagella in a small percentage of the cells.

Live cell microscopy and image analysis

For TIRF microscopy, 15 µl of cells in TAP media were applied to cover glass (22 mm × 22 mm; Corning) and inverted onto slides (Gold Seal; Thermo Fisher Scientific) with a square petroleum jelly spacer. Images were acquired at room temperature with NIS-Elements software (version 2.3; Nikon) on an inverted microscope (TE2000-E; Nikon) equipped with a through the objective TIRF system, the Perfect Focus system (Nikon), 100×/1.49 NA and 60×/1.45 NA Apo TIRF oil immersion objectives (Nikon), and a cooled EM charge-coupled device (CCD) camera (QuantEM:512SC; Photometrics) with quantitative gain. Cells were imaged at ∼30 frames per second with adjusted TIRF, where the angle of incident light is slightly decreased from the supercritical range toward the critical angle, allowing a deeper range of observation in the area near the cover glass. The depth of illumination was measured to be ∼250–350 nm using 6-µm fluorescent beads as described previously by Mattheyses and Axelrod (2006). All images in each imaging session were acquired using the same angle of incidence, and efforts were taken to replicate incidence angles between imaging sessions (although some variability occurred, e.g., see Fig. S1 D). GFP was imaged with 488-nm excitation and a 525/50 emission filter.

For DIC imaging, 10 µl of wild-type cells was immobilized between a 0.25% agarose/TAP pad and the cover glass. The cover glass was sealed to the slide with VALAP (equal parts petroleum jelly, lanolin, and paraffin) to prevent dehydration. Images were acquired at room temperature with NIS-Elements on an inverted scope (TE2000-E) with a 0.85 NA dry condenser, a 100×/1.4 NA oil objective (Nikon), and a cooled CCD camera (CoolSNAP HQ^2 interline; Photometrics).

Kymographs of both the TIRF and DIC imaging were generated with Metamorph software (version 7.5.1.0; MDS Analytical Technologies) by drawing a box along the length of the flagella with a width slightly greater than that of the flagella. The maximum intensity value (for TIRF) or average intensity (for DIC) for each point along the length of the box was plotted for each frame in the video, yielding kymographs with spatial information along the x axis and time along the y axis. Using NIS-Elements, kymographs were analyzed for average IFT train intensity, speed, frequency, and integrated flagellar intensity (Fig. S1 B). Intensity measurements were normalized for either camera noise or flagellar background signal. Camera noise was measured as the mean value of an ROI on the kymographs outside of the flagellar region. Flagellar background was measured as the

average minimum value of several ROIs placed within the center of each flagellar region.

For the regeneration kinetics in Fig. 1 A, cells were fixed every 5 min after pH shock and immediately imaged with an upright Axio Scope (Carl Zeiss, Inc.), a 40×/.75 NA air objective (Carl Zeiss, Inc.), and a CCD camera (SPOT; model 1.4.0; Digital Instruments). Flagellar lengths at each time point were measured using NIS-Elements.

Fixed-cell photobleaching and step analysis

At various time points after pH shock, 100 µl of cells was plated onto cover glass and fixed with formaldehyde (4% final concentration) for 10 min shielded from the light. Cells were fixed after plating to preserve flagellar adhesion to the cover glass. The cover glass was dipped in PBS to remove unadhered cells, mounted onto slides with 10 µl PBS and a petroleum jelly spacer, and sealed with VALAP. Flagella were bleached with the same adjusted TIRF illumination that was used for live cell imaging. Time series (~20 frames per second) were acquired immediately after locating cells to ensure that the maximal number of bleaching events was recorded.

Mean intensity plots for individual trains were generated in NIS-Elements from square ROIs (0.416 × 0.416 µm) corresponding to points of peak intensity along the flagella. Steps were enhanced by filtering the raw data with an edge-preserving Chung-Kennedy algorithm, which passes two adjacent sliding windows of adjustable width (20–60 frames/window) over the dataset and outputs the mean of the window with the lower variance (Leake et al., 2006). Although every step was not always clear, each intensity plot contained numerous steps of roughly the same size from which the rest of the steps could be estimated. The number of bleaching events counted by eye was rechecked for each plot by dividing the total change in intensity by the average step size. The geometry of the axoneme in relation to the TIRF field did increase step size variability, as GFP proteins further from the cover glass were less intense and less likely to photobleach, yielding smaller steps toward the end of the bleach (Fig. 2 B). Importantly, when the whole dataset was plotted together, the total change in intensity of the ROIs was tightly correlated with the number of GFP steps counted, validating the accuracy of the step quantification (Fig. S1 D). However, the estimated number of KAP-GFP proteins per train may have been slightly inflated because train bleaching events were inseparable from the flagellar background.

Isolation of flagella and Western blotting

Flagella were isolated by pH shock and centrifugation onto a 25% sucrose cushion as described previously in Cole et al. (1998). Western blots were probed with rat anti-KAP antibody (provided by M. Porter; Mueller et al., 2005) at 1:5,000 and goat anti–rat HRP secondary antibody (Jackson ImmunoResearch Laboratories) at 1:20,000.

Online supplemental material

Fig. S1 shows imaging and photobleaching controls. Fig. S2 shows IFT speed, frequency, and intensity correlations from the pH shock experiment (Fig. 1). Fig. S3 shows the complete raw and normalized datasets from the long-zero experiment (Fig. 3), corrected for camera noise instead of flagellar background. Videos 1–6 show KAP-GFP and IFT27-GFP cells from the pH shock and long-zero experiments. Online supplemental material is available at http://www.jcb.org/cgi/content/full/jcb.200812084/DC1.

We thank Kurt Thorn and the Nikon Imaging Center at the University of California San Francisco for invaluable microscopy resources and assistance. We also thank Joshua Mueller, Mary Porter, Hongmin Qin, Joel Rosenbaum, Karl Lechtreck, and George Witman for generously sharing strains and antibodies, as well as Orion Weiner, Bruce Alberts, Susanne Rafelski, Lani Keller, Sarah Goodwin, and the Marshall Laboratory for helpful discussions and careful reading of the manuscript. B.D. Engel planned and conducted the experiments, analyzed the results, and wrote the paper. W.B. Ludington conceived the strategy of quantifying IFT using KAP-GFP and suggested the pH shock and long-zero experiments, whereas B.D. Engel devised the approach of using TIRF imaging and kymographs to acquire and analyze the data. W.F. Marshall supervised the project, suggested controls and analyses, and helped with writing the paper.

This work was funded by the W.M. Keck Foundation Distinguished Young Scholars Program (W.F. Marshall), the Searle Scholar Program (W.F. Marshall), the Genentech Graduate Fellowship (B.D. Engel), and the National Science Foundation Graduate Research Fellowship (W.B. Ludington).

Submitted: 15 December 2008
Accepted: 1 July 2009

References

Absalon, S., T. Blisnick, L. Kohl, G. Toutirais, G. Doré, D. Julkowska, A. Tavenet, and P. Bastin. 2008. Intraflagellar transport and functional analysis of genes required for flagellum formation in trypanosomes. *Mol. Biol. Cell.* 19:929–944. doi:10.1091/mbc.E07-08-0749

Asleson, C.M., and P.A. Lefebvre. 1998. Genetic analysis of flagellar length control in *Chlamydomonas reinhardtii*: a new long-flagella locus and extragenic suppressor mutations. *Genetics.* 148:693–702.

Axelrod, D. 2001. Total internal reflection fluorescence microscopy in cell biology. *Traffic.* 2:764–774. doi:10.1034/j.1600-0854.2001.21104.x

Baker, S.A., K. Freeman, K. Luby-Phelps, G.J. Pazour, and J.C. Besharse. 2003. IFT20 links kinesin II with a mammalian intraflagellar transport complex that is conserved in motile flagella and sensory cilia. *J. Biol. Chem.* 278:34211–34218. doi:10.1074/jbc.M300156200

Berman, S.A., N.F. Wilson, N.A. Haas, and P.A. Lefebvre. 2003. A novel MAP kinase regulates flagellar length in *Chlamydomonas. Curr. Biol.* 13:1145–1149. doi:10.1016/S0960-9822(03)00415-9

Bisgrove, B.W., and H.J. Yost. 2006. The roles of cilia in developmental disorders and disease. *Development.* 133:4131–4143. doi:10.1242/dev.02595

Bloodgood, R.A. 1995. Flagellar surface motility: gliding and microsphere movements. *Methods Cell Biol.* 47:273–279. doi:10.1016/S0091-679X(08)60820-1

Bradley, B.A., and L.M. Quarmby. 2005. A NIMA-related kinase, Cnk2p, regulates both flagellar length and cell size in *Chlamydomonas. J. Cell Sci.* 118:3317–3326. doi:10.1242/jcs.02455

Chung, S.H., and R.A. Kennedy. 1991. Forward-backward non-linear filtering technique for extracting small biological signals from noise. *J. Neurosci. Methods.* 40:71–86. doi:10.1016/0165-0270(91)90118-J

Cole, D.G. 2003. The intraflagellar transport machinery of *Chlamydomonas reinhardtii. Traffic.* 4:435–442. doi:10.1034/j.1600-0854.2003.t01-1-00103.x

Cole, D.G., D.R. Diener, A.L. Himelblau, P.L. Beech, J.C. Fuster, and J.L. Rosenbaum. 1998. *Chlamydomonas* kinesin-II-dependent intraflagellar transport (IFT): IFT particles contain proteins required for ciliary assembly in *Caenorhabditis elegans* sensory neurons. *J. Cell Biol.* 141:993–1008. doi:10.1083/jcb.141.4.993

Deacon, S.W., A.S. Serpinskaya, P.S. Vaughan, M. Lopez Fanarraga, I. Vernos, K.T. Vaughan, and V.I. Gelfand. 2003. Dynactin is required for bidirectional organelle transport. *J. Cell Biol.* 160:297–301. doi:10.1083/jcb.200210066

Deane, J.A., D.G. Cole, E.S. Seeley, D.R. Diener, and J.L. Rosenbaum. 2001. Localization of intraflagellar transport protein IFT52 identifies basal body transitional fibers as the docking site for IFT particles. *Curr. Biol.* 11:1586–1590.

Dentler, W. 2005. Intraflagellar transport (IFT) during assembly and disassembly of *Chlamydomonas* flagella. *J. Cell Biol.* 170:649–659. doi:10.1083/jcb.200412021

Follit, J.A., R.A. Tuft, K.E. Fogarty, and G.J. Pazour. 2006. The intraflagellar transport protein IFT20 is associated with the Golgi complex and is required for cilia assembly. *Mol. Biol. Cell.* 17:3781–3792. doi:10.1091/mbc.E06-02-0133

Fuhrmann, M., W. Oertel, and P. Hegemann. 1999. A synthetic gene coding for the green fluorescent protein (GFP) is a versatile reporter in *Chlamydomonas reinhardtii. Plant J.* 19:353–361. doi:10.1046/j.1365-313X.1999.00526.x

Gorman, D.S., and R.P. Levine. 1965. Cytochrome f and plastocyanin: their sequence in the photosynthetic electron transport chain of *Chlamydomonas reinhardi. Proc. Natl. Acad. Sci. USA.* 54:1665–1669. doi:10.1073/pnas.54.6.1665

Hou, Y., H. Qin, J.A. Follit, G.J. Pazour, J.L. Rosenbaum, and G.B. Witman. 2007. Functional analysis of an individual IFT protein: IFT46 is required for transport of outer dynein arms into flagella. *J. Cell Biol.* 176:653–665. doi:10.1083/jcb.200608041

Huang, B., M.R. Rifkin, and D.J. Luck. 1977. Temperature-sensitive mutations affecting flagellar assembly and function in *Chlamydomonas reinhardtii. J. Cell Biol.* 72:67–85. doi:10.1083/jcb.72.1.67

Iomini, C., V. Babaev-Khaimov, M. Sassaroli, and G. Piperno. 2001. Protein particles in *Chlamydomonas* flagella undergo a transport cycle consisting of four phases. *J. Cell Biol.* 153:13–24. doi:10.1083/jcb.153.1.13

Kozminski, K.G., K.A. Johnson, P. Forscher, and J.L. Rosenbaum. 1993. A motility in the eukaryotic flagellum unrelated to flagellar beating. *Proc. Natl. Acad. Sci. USA.* 90:5519–5523. doi:10.1073/pnas.90.12.5519

Kozminski, K.G., P.L. Beech, and J.L. Rosenbaum. 1995. The *Chlamydomonas* kinesin-like protein FLA10 is involved in motility associated with the flagellar membrane. *J. Cell Biol.* 131:1517–1527. doi:10.1083/jcb.131.6.1517

Kuchka, M.R., and J.W. Jarvik. 1987. Short-flagella mutants of *Chlamydomonas reinhardtii. Genetics.* 115:685–691.

Leake, M.C., J.H. Chandler, G.H. Wadhams, F. Bai, R.M. Berry, and J.P. Armitage. 2006. Stoichiometry and turnover in single, functioning membrane protein complexes. *Nature.* 443:355–358. doi:10.1038/nature05135

Lefebvre, P.A. 1995. Flagellar amputation and regeneration in *Chlamydomonas. Methods Cell Biol.* 47:3–7. doi:10.1016/S0091-679X(08)60782-7

Marshall, W.F., and J.L. Rosenbaum. 2001. Intraflagellar transport balances continuous turnover of outer doublet microtubules: implications for flagellar length control. *J. Cell Biol.* 155:405–414. doi:10.1083/jcb.200106141

Marshall, W.F., H. Qin, M. Rodrigo Brenni, and J.L. Rosenbaum. 2005. Flagellar length control system: testing a simple model based on intraflagellar transport and turnover. *Mol. Biol. Cell.* 16:270–278. doi:10.1091/mbc.E04-07-0586

Mattheyses, A.L., and D. Axelrod. 2006. Direct measurement of the evanescent field profile produced by objective-based total internal reflection fluorescence. *J. Biomed. Opt.* 11:014006. doi:10.1117/1.2161018

Mueller, J., C.A. Perrone, R. Bower, D.G. Cole, and M.E. Porter. 2005. The FLA3 KAP subunit is required for localization of kinesin-2 to the site of flagellar assembly and processive anterograde intraflagellar transport. *Mol. Biol. Cell.* 16:1341–1354. doi:10.1091/mbc.E04-10-0931

Müller, M.J., S. Klumpp, and R. Lipowsky. 2008. Tug-of-war as a cooperative mechanism for bidirectional cargo transport by molecular motors. *Proc. Natl. Acad. Sci. USA.* 105:4609–4614. doi:10.1073/pnas.0706825105

Orozco, J.T., K.P. Wedaman, D. Signor, H. Brown, L. Rose, and J.M. Scholey. 1999. Movement of motor and cargo along cilia. *Nature.* 398:674. doi:10.1038/19448

Ou, G., M. Koga, O.E. Blacque, T. Murayama, Y. Ohshima, J.C. Schafer, C. Li, B.K. Yoder, M.R. Leroux, and J.M. Scholey. 2007. Sensory ciliogenesis in *Caenorhabditis elegans*: assignment of IFT components into distinct modules based on transport and phenotypic profiles. *Mol. Biol. Cell.* 18:1554–1569. doi:10.1091/mbc.E06-09-0805

Pan, J., and W.J. Snell. 2005. *Chlamydomonas* shortens its flagella by activating axonemal disassembly, stimulating IFT particle trafficking, and blocking anterograde cargo loading. *Dev. Cell.* 9:431–438. doi:10.1016/j.devcel.2005.07.010

Parker, J.D., and L.M. Quarmby. 2003. *Chlamydomonas* fla mutants reveal a link between deflagellation and intraflagellar transport. *BMC Cell Biol.* 4:11. doi:10.1186/1471-2121-4-11

Patterson, G.H., and J. Lippincott-Schwartz. 2002. A photoactivatable GFP for selective photolabeling of proteins and cells. *Science.* 297:1873–1877. doi:10.1126/science.1074952

Pazour, G.J., and J.L. Rosenbaum. 2002. Intraflagellar transport and cilia-dependent diseases. *Trends Cell Biol.* 12:551–555. doi:10.1016/S0962-8924(02)02410-8

Pazour, G.J., B.L. Dickert, and G.B. Witman. 1999. The DHC1b (DHC2) isoform of cytoplasmic dynein is required for flagellar assembly. *J. Cell Biol.* 144:473–481. doi:10.1083/jcb.144.3.473

Pazour, G.J., B.L. Dickert, Y. Vucica, E.S. Seeley, J.L. Rosenbaum, G.B. Witman, and D.G. Cole. 2000. *Chlamydomonas* IFT88 and its mouse homologue, polycystic kidney disease gene tg737, are required for assembly of cilia and flagella. *J. Cell Biol.* 151:709–718.

Pedersen, L.B., M.S. Miller, S. Geimer, J.M. Leitch, J.L. Rosenbaum, and D.G. Cole. 2005. *Chlamydomonas* IFT172 is encoded by FLA11, interacts with CrEB1, and regulates IFT at the flagellar tip. *Curr. Biol.* 15:262–266. doi:10.1016/j.cub.2005.01.037

Pedersen, L.B., S. Geimer, and J.L. Rosenbaum. 2006. Dissecting the molecular mechanisms of intraflagellar transport in *chlamydomonas. Curr. Biol.* 16:450–459. doi:10.1016/j.cub.2006.02.020

Pigino, G., S. Geimer, S. Lanzavecchia, E. Paccagnini, F. Cantele, D.R. Diener, J.L. Rosenbaum, and P. Lupetti. 2009. Electron-tomographic analysis of intraflagellar transport particle trains in situ. *J. Cell Biol.* 187:135–148.

Piperno, G., and K. Mead. 1997. Transport of a novel complex in the cytoplasmic matrix of *Chlamydomonas* flagella. *Proc. Natl. Acad. Sci. USA.* 94:4457–4462. doi:10.1073/pnas.94.9.4457

Piperno, G., E. Siuda, S. Henderson, M. Segil, H. Vaananen, and M. Sassaroli. 1998. Distinct mutants of retrograde intraflagellar transport (IFT) share similar morphological and molecular defects. *J. Cell Biol.* 143:1591–1601. doi:10.1083/jcb.143.6.1591

Porter, M.E., R. Bower, J.A. Knott, P. Byrd, and W. Dentler. 1999. Cytoplasmic dynein heavy chain 1b is required for flagellar assembly in *Chlamydomonas. Mol. Biol. Cell.* 10:693–712.

Qin, H., D.R. Diener, S. Geimer, D.G. Cole, and J.L. Rosenbaum. 2004. Intraflagellar transport (IFT) cargo: IFT transports flagellar precursors to the tip and turnover products to the cell body. *J. Cell Biol.* 164:255–266. doi:10.1083/jcb.200308132

Qin, H., Z. Wang, D. Diener, and J.L. Rosenbaum. 2007. Intraflagellar transport protein 27 is a small G protein involved in cell-cycle control. *Curr. Biol.* 17:193–202. doi:10.1016/j.cub.2006.12.040

Randall, J., H.R. Munden, and P.H. Prest. 1969. The flagellar apparatus as a model organelle for the study of growth and morphopoiesis. With an appendix. Temperature control apparatus used in flagellar regeneration experiments. *Proc R Soc Lond B Biol Sci.* 173:31–62, passimdoi:10.1098/rspb.1969.0034.

Rosenbaum, J.L. 2003. Organelle size regulation: length matters. *Curr. Biol.* 13:R506–R507. doi:10.1016/S0960-9822(03)00440-8

Rosenbaum, J.L., J.E. Moulder, and D.L. Ringo. 1969. Flagellar elongation and shortening in *Chlamydomonas*. The use of cycloheximide and colchicine to study the synthesis and assembly of flagellar proteins. *J. Cell Biol.* 41:600–619. doi:10.1083/jcb.41.2.600

Silflow, C.D., and P.A. Lefebvre. 2001. Assembly and motility of eukaryotic cilia and flagella. Lessons from *Chlamydomonas reinhardtii. Plant Physiol.* 127:1500–1507. doi:10.1104/pp.010807

Sloboda, R.D., and L. Howard. 2007. Localization of EB1, IFT polypeptides, and kinesin-2 in *Chlamydomonas* flagellar axonemes via immunogold scanning electron microscopy. *Cell Motil. Cytoskeleton.* 64:446–460. doi:10.1002/cm.20195

Sloboda, R.D., and J.L. Rosenbaum. 2007. Making sense of cilia and flagella. *J. Cell Biol.* 179:575–582. doi:10.1083/jcb.200709039

Smith, D.A. 1998. A quantitative method for the detection of edges in noisy time-series. *Philos. Trans. R. Soc. Lond. B Biol. Sci.* 353:1969–1981. doi:10.1098/rstb.1998.0348

Snell, W.J., J. Pan, and Q. Wang. 2004. Cilia and flagella revealed: from flagellar assembly in *Chlamydomonas* to human obesity disorders. *Cell.* 117:693–697. doi:10.1016/j.cell.2004.05.019

Tsao, C.C., and M.A. Gorovsky. 2008. Different effects of *Tetrahymena* IFT172 domains on anterograde and retrograde intraflagellar transport. *Mol. Biol. Cell.* 19:1450–1461. doi:10.1091/mbc.E07-05-0403

Wilson, N.F., and P.A. Lefebvre. 2004. Regulation of flagellar assembly by glycogen synthase kinase 3 in *Chlamydomonas reinhardtii. Eukaryot. Cell.* 3:1307–1319. doi:10.1128/EC.3.5.1307-1319.2004